

High-Throughput Flexible Belief Propagation List Decoder for Polar Codes

Yuqing Ren, Yifei Shen, Leyu Zhang, Andreas Toftegaard Kristensen, Alexios

Balatsoukas-Stimming, *Member, IEEE*, Andreas Burg, *Senior Member, IEEE*, Chuan Zhang, *Senior Member, IEEE*

Abstract—Due to its high parallelism, belief propagation (BP) decoding can be implemented with high throughput and is a promising solution to meet the ultra-high peak data rate requirement of future communication systems. However, for polar codes, the error-correcting performance of BP decoding is far inferior to that of widely used CRC-aided successive cancellation list (SCL) decoding algorithm. To close the performance gap to SCL, BP list (BPL) decoding expands the exploration of candidate codewords through multiple permuted factor graphs (PFGs). From an implementation perspective, designing a unified and flexible hardware architecture of BPL decoding that supports different PFGs and various code configurations is challenging. In this paper, we propose the first hardware implementation of a BPL decoder for polar codes and overcome the implementation challenge by applying a hardware-friendly algorithm that generates flexible permutations on the fly. First, we derive the permutation selection gain and provide a sequential generation (SG) algorithm to obtain a near-optimal PFG set. We further prove that any permutation can be decomposed into a combination of multiple fixed routings, and we design a low-complexity permutation network to satisfy the decoding schedule. Our BPL decoder not only has a low decoding latency by executing the decoding and permutation generation in parallel, but also supports an arbitrary list size without any area overhead. Experimental results show that, for length-1024 polar codes with a code of one-half, our BPL decoder with a list size $L = 32$ has a similar error-correcting performance to SCL with $L = 4$ and achieves a throughput of 25.63 Gbps and an area efficiency of 29.46 Gbps/mm² at SNR = 4.0 dB, which is 1.99× and 7.08× faster than the state-of-the-art BP flip and SCL decoders, respectively.

Index Terms—polar codes, high-throughput, belief propagation list (BPL) decoding, permuted factor graph, permutation, automorphism ensemble, hardware implementation.

I. INTRODUCTION

POLAR codes, proposed by Arikan in [1], have become an integral part of 5G new radio (NR), where they were ratified as the standard codes for the control channels of 5G enhanced mobile broadband (eMBB) scenarios [2]. Along with the invention of polar codes, Arikan introduced successive cancellation (SC) decoding and belief propagation (BP) decoding. Following the evolution of communication scenarios, both SC and BP decoding led the development of polar decoding algorithms and implementations, which were extended into a series of advanced polar decoders such as

SC list (SCL) [3]–[9], BP list (BPL) [10]–[18], and BP flip (BPF) [19]–[22] decoders.

While the original SC decoding algorithm can achieve channel capacity at infinite code lengths, it shows poor error-correcting performance with practical finite code lengths. To improve the error-correcting performance of SC decoding, SCL decoding was proposed in [3] to keep a list of up to L candidate codewords. Additionally, when concatenated with cyclic redundancy check (CRC) codes [4], polar codes with SCL decoding outperform low-density parity-check (LDPC) and Turbo codes in terms of the error-correcting performance [23]. To satisfy the low-latency and high throughput requirements of eMBB scenarios, node-based fast SCL decoders [5]–[9] focus on exploiting special constituent codes [24]–[28], which help to avoid traversing the lower stages of the decoding tree to provide a significant reduction in decoding latency compared to conventional bit-wise SCL decoders. The state-of-the-art (SOA) node-based SCL decoder [9] with a list size ($L = 8$) achieves a throughput of more than 2.94 Gbps, which fits the reliability, latency, and throughput requirements of eMBB scenarios. However, when considering the ultra-high peak data rate requirements of future communication systems [29], SC-based decoders become impractical due to the serial processing inherent in these algorithms [5]–[9].

In contrast to SC-based decoding, BP decoding is an inherently parallel algorithm. BP decoding can therefore be implemented easily in a multi-stage factor graph in pursuit of a much higher throughput [30]. Additionally, BP decoding has the potential to realize iterative detection and decoding to achieve better system performance than separate detection and decoding [31], [32], which further raises the interest in BP decoding for academia and industry. Though the error-correcting performance of BP decoding improves as the iteration number increases, it is still far behind the SCL performance. BPF decoding [19]–[22] and BPL decoding [10]–[18] are two advanced BP algorithms that can approach the performance of SCL by expanding the exploration of candidate codewords. BPF decoding guesses the positions of error-prone bits and sequentially corrects them in additional decoding attempts. Unfortunately, online identification of error-prone bits [20]–[22] through sorting and post-processing of channel messages increases the hardware complexity and degrades the maximum operating frequency [22]. Alternatively, BPL decoding proposed in [11] tries to decode on multiple permuted factor graphs (PFGs), where the number of possible PFGs is $n!$ ($n = \log_2 N$) for length- N polar codes. Decoding schedules of BPL can be divided into parallel [11]–[14] and serial schedules [17], respectively. In parallel BPL decoding, L independent BP decoders operate in parallel (each BP decoder

Y. Ren, Y. Shen, A. T. Kristensen, and A. Burg are with the Telecommunications Circuits Laboratory (TCL), École Polytechnique Fédérale de Lausanne (EPFL), Lausanne 1015, Switzerland (email: {yuqing.ren, yifei.shen, andreas.kristensen, andreas.burg}@epfl.ch). *Corresponding author: Andreas Burg.*

Y. Shen, L. Zhang and C. Zhang are with the LEADS of Southeast University, the National Mobile Communications Research Laboratory, and the Purple Mountain Laboratories, Nanjing 210096, China (email: chzhang@seu.edu.cn).

A. Balatsoukas-Stimming is with the Department of Electrical Engineering, Eindhoven University of Technology, 5600 MB Eindhoven, The Netherlands (email: a.k.balatsoukas.stimming@tue.nl).

works on a unique PFG) and the optimal codeword with the minimum Euclidean distance to the received signals is selected from the \mathbb{L} identified candidate codewords. However, parallel BPL decoding has very poor hardware utilization, especially for large list sizes. To avoid the high hardware consumption caused by the parallel architecture, the authors of [17] proposed a serial BPL decoding schedule, in which shuffling the input LLRs can be substituted for permutations of the factor graph stages. This hardware-friendly decoding strategy allows BPL decoding to reuse a single BP decoder at the cost of merely shuffling the input LLRs into a specific order for each PFG.

To improve the error-correcting performance of BPL decoding, numerous researchers have explored methods of optimizing the PFG selection, including empirical methods [11], [17], [33] and analytical methods [14]–[16]. It is noteworthy that the authors of [14] first derived the permutation gain for parallel BPL decoding, which provides the inspiration for analytically solving the optimal PFG selection. In view of hardware implementations, many works of BP decoders have been presented in [30], [34]–[39]. Compared to the classical single-column BP architectures [30], the SOA double-column bidirectional-propagation architecture [39] instantiates two processing element (PE) arrays and propagates the left-to-right and right-to-left messages simultaneously to improve the throughput. Moreover, the most challenging task for the BPL decoder is the implementation of flexible permutations since the PFG selection algorithms [14]–[16], [40] are generally dynamic, corresponding to varying code configurations or channel environments. Even if based on area-efficient serial decoding, the BPL decoder still needs to support the generation of flexible permutations by shuffling the input LLRs into a specific order for each PFG. A straightforward method is to utilize the Beneš network [41], [42], which is an optimal non-blocking network that can achieve any arbitrary permutation. However, the design space of permutations is $n!$ instead of $N!$ for length- N polar codes, and the control signals of the Beneš network are difficult to generate on the fly for each PFG. It is not efficient to adopt the Beneš network in the BPL decoder. In summary, there are thus two critical problems for the BPL decoder:

- How to select the optimal PFG set from $n!$ PFGs for length- N polar codes?
- How to efficiently implement flexible permutations for BPL decoding in hardware?

It is further noteworthy that BPL decoding is a particular case of a generalized automorphism ensemble (AE) decoding, in which we can deploy the SC, SCL, or BP decoding on multiple PFGs to achieve ML performance of polar or Reed-Muller (RM) codes [43], [44]. Hence, the solutions to these two problems are significant for both BPL and for generalized AE decoding.

Contributions:

In this paper, we present the first BPL implementation, which solves the aforementioned two problems, i.e., the use of near-optimal PFG sets and the generation of flexible permutations. Our contributions comprise the following:

- We derive the block error probability of serial BPL decoding and present an explicit criterion for the best PFG set. Then, we propose a sequential generation (SG)

algorithm to obtain a near-optimal PFG set. Simulations show that our BPL decoder with $\mathbb{L} = 32$ achieves a similar error-correcting performance to SCL with $\mathbb{L} = 4$.

- We propose a hardware-friendly algorithm using low-complexity matrix decomposition to generate flexible permutation routings for all PFGs. To this end, we provide a mathematical model for permutations and prove that the permutation routing of each PFG can be decomposed into a combination of $n - 1$ fixed sub-routings. This decomposition process can be done online.
- We present the first hardware architecture of a BPL decoder. Based on the SOA double-column bidirectional-propagation architecture [39], we implement the aforementioned flexible permutation generator. Moreover, a decoupled strategy for executing BP decoding and permutation generation simultaneously is adopted to improve the throughput of the BPL decoder significantly. It is noteworthy that our decoder can arbitrarily increase the list size without any additional area overhead. Synthesis results show that, for $\mathbb{L} = 32$, our decoder can achieve a throughput of 25.63 Gbps with an area efficiency of 29.46 Gbps/mm² at SNR = 4 dB, which outperforms the SOA BP and BPF decoders [20], [21], [38], [39], [45].

The remainder of this paper is organized as follows. Section II reviews the background of polar codes, BP decoding, and BPL decoding. Section III analyses the permutation gain for serial BPL decoding and presents a graph selection algorithm for a near-optimal PFG set. In Section IV, a hardware-friendly algorithm for any permutation generation is proposed. Section V presents our BPL decoder architecture with several advanced techniques. Section VI provides our implementation results and compares them with the SOA polar decoders. Finally, Section VII concludes this paper.

II. PRELIMINARIES

Notation: Throughout this paper, we use the following symbol definitions. Boldface lowercase letters \mathbf{u} denote vectors, where u_i means the i -th element of \mathbf{u} and \mathbf{u}_i^j denotes the sub-vector $[u_i u_{i+1} \cdots u_j]$, $i \leq j$. If $i > j$, $\mathbf{u}_i^j = \emptyset$. Boldface uppercase letters \mathbf{B} denote matrices, where B_{ij} and \mathbf{b}_j denote the element at the i -th row and j -th column of \mathbf{B} and the j -th column of \mathbf{B} , respectively. In terms of the factor graph for polar codes with length $N = 2^n$, we use $\pi_0, [m_0 m_1 m_2 \cdots m_{n-1}]$, and $[0 1 2 \cdots n - 1]$ to represent the original factor graph (OFG), its stages, and its stage order, respectively. Similarly, we use $\pi, [m_{\pi^0} m_{\pi^1} m_{\pi^2} \cdots m_{\pi^{n-1}}]$, and $[\pi^0 \pi^1 \pi^2 \cdots \pi^{n-1}]$ to denote any other PFG, its stages, and its stage order, respectively. If \mathcal{L} is a countable set of \mathbb{L} PFG candidates, $\{\tilde{\pi}_0 \tilde{\pi}_1 \cdots \tilde{\pi}_{\mathbb{L}-1}\}$, $|\mathcal{L}| = \mathbb{L}$ means its cardinality. Note that all indices related to decoding start from 0. The function $\text{HD}(x) := 1_{x < 0}$ defines the hard decision function. We adopt the following parameters for polar codes, N is the code length, K is the number of information bits, $R = K/N$ the code-rate, P the number of CRC bits, $K' = K + P$ the number of message bits with the CRC bits attached. The frozen and unfrozen bit set indices are denoted as \mathcal{F} and \mathcal{A} , respectively, and we refer to a code as an (N, K) polar code.

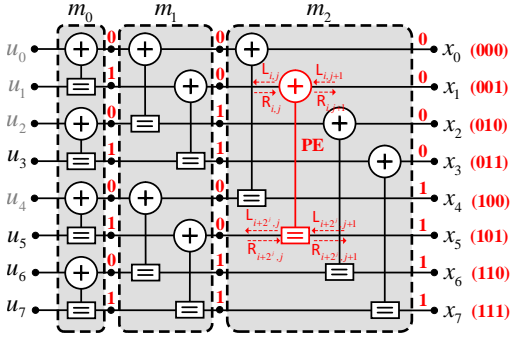


Fig. 1. The OFG for length-8 polar codes, where one PE is marked in red and $\mathcal{F} = \{0, 1, 2, 4\}$ is marked in grey.

A. Construction and Encoding of Polar Codes

Given an input bit sequence \mathbf{u} , the encoded vector \mathbf{x} is generated by $\mathbf{x} = \mathbf{u} \cdot \mathbf{G}_N$, where $\mathbf{G}_N = \mathbf{F}^{\otimes n}$ denotes the Kronecker power of the kernel $\mathbf{F} = \begin{bmatrix} 1 & 0 \\ 1 & 1 \end{bmatrix}$. Based on the principle of channel polarization [1], the N bits in \mathbf{u} correspond to N coordinated bit channels with different reliabilities, where the K' most reliable bit channels transmit unfrozen bits with CRC attached and the remaining $N - K'$ bit channels transmit frozen bits, typically set to a value of 0. Note that the metric used to determine the bit channel reliability has an impact on \mathcal{A} and influences the performance of polar codes. For 5G NR [46], a universal reliability sequence is applied to formulate \mathcal{A} with K' bits for uplink (UL) and downlink (DL) channels. Besides, a novel polar code construction framework tailored to a given decoding algorithm based on a genetic algorithm (GenAlg) was introduced in [47], where populations of unfrozen sets evolve based on the error-correcting performance of a given decoder.

B. BP Decoding of Polar Codes on the Factor Graph

The BP algorithm is a classical iterative algorithm to calculate the marginal probability by the sum-product (SP) equations on a factor graph [48]. Motivated by BP decoding for RM codes, Arikan first proposed BP decoding for polar codes on the generator matrix-based factor graph [49]. The OFG structure with three stages $[m_0 \ m_1 \ m_2]$ is shown in Fig. 1. Namely, an (N, K) polar code is represented as an n -stage factor graph, and each stage has $N/2$ PEs. Two types of LLR messages (left-to-right R and right-to-left L) are propagated over PEs on the factor graph. For $j = 0, \dots, n$, R_j and L_j can be denoted as the j -th column of R- and L-messages, respectively, where $R_{i,j}$ and $L_{i,j}$ denote the messages at the i -th bit index of the j -th column, respectively. Each PE propagates R- and L-messages as follows

$$\begin{cases} L_{i,j} = g(L_{i,j+1}, L_{i+2^j,j+1} + R_{i+2^j,j}, \beta_L), \\ L_{i+2^j,j} = g(L_{i,j+1}, R_{i,j}, \beta_L) + L_{i+2^j,j+1}, \\ R_{i,j+1} = g(R_{i,j}, L_{i+2^j,j+1} + R_{i+2^j,j}, \beta_R), \\ R_{i+2^j,j+1} = g(R_{i,j}, L_{i,j+1}, \beta_R) + R_{i+2^j,j}. \end{cases} \quad (1)$$

where we adopt the offset-MS (OMS) equation [20], [50] to approximate the SP equation for all iterative BP decoders. It can be implemented easily in hardware to approach the performance of the SP, where $g(a, b, \beta) = \text{sgn}(a) \cdot \text{sgn}(b) \cdot \max(\min(|a|, |b|) - \beta, 0)$ and $[\beta_R \ \beta_L] = [0.25 \ 0]$.

At the beginning of BP decoding, R_0 is initialized as *a-priori*

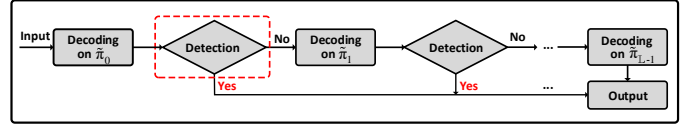


Fig. 2. Overall framework for serial BPL decoding with the detection.

$+\infty$ or 0 according to the bit channel allocation of \mathcal{F} and L_n is initialized as *a-posteriori* LLR values from the received signals \mathbf{y} , i.e., $\ln \frac{\Pr(y_i | x_i=0)}{\Pr(y_i | x_i=1)}$, $0 \leq i \leq N - 1$. R- and L-messages of other stages on the factor graph are initialized as 0. When the maximum number of iteration I_{\max} is reached, the HD results $\hat{\mathbf{u}}$ are estimated based on the decision LLRs ($R_0 + L_0$).

C. BPL Decoding of Polar Codes

BPL decoding [11] is an efficient algorithm to enhance the error-correcting performance of BP decoding, which executes multiple BP decoding procedures on multiple PFGs either in parallel [11]–[14] or serially [17]. Parallel BPL decoding instantiates a set \mathcal{L} of \mathbb{L} independent BP decoders (each BP decoder works on a unique PFG), which leads to a poor hardware utilization since only one result is finally retained. Alternatively, serial BPL decoding can reuse a single BP decoder, which is illustrated in Fig. 2. If one BP decoding attempt does not pass the detection within I_{\max} , serial BPL decoding activates the decoding on next PFG. Note that, due to the detection in Fig. 2, the miss, false-alarm, and error-detection events of each PFG are introduced, which are denoted as M , F , and D , respectively.¹ In the following, all BPL decoders are used on the serial structure unless stated otherwise. Moreover, in terms of the PFG selection, we note that previous works have found that the OFG always yields the best error-correcting performance [14] and the PFGs which fix more left stages and only permute the right-most side of the graph can have a better error-correcting performance [17]. This can be done as follows

$$[m_0 \ m_1 \ \dots \ m_{p-1} \ m_{\pi p} \ \dots \ m_{\pi^{n-1}}], \quad 0 \leq p \leq n, \quad (2)$$

where p denotes the number of fixed left stages. Note that the size of the design space of PFGs is simplified as $(n - p)!$, which facilitates our derivations in Section III.

D. Permutation by Shuffling the Input LLRs

A one-to-one mapping exists between permutation of the factor graph stages and shuffling of the positions of the bits in the codeword [17]. If we consider a node \oplus as a ‘0’ and a node \boxminus as a ‘1’ on the factor graph, we can derive the ‘0/1’ sequences that describe the factor graph from the binary expansion of the bit-index i for u_i and x_i , as shown in the OFG of Fig. 1. Subsequently, Fig. 3 depicts the permutation of a PFG $\pi_1 = [m_2 \ m_0 \ m_1]$ based on the input shuffling. Note that, by permuting the stages of the factor graph, the positions of the nodes \oplus and \boxminus have been changed, i.e., the binary expansions of the bit indices for the input LLRs also have been changed. We can instantiate a routing based on these binary expansions to shuffle the input LLRs, which

¹ M represents a wrong codeword which passes the detection, F represents a correct codeword which fails to pass the detection, and D is a codeword which is detected as wrong. We generally use a CRC detection as the detection strategy in serial BPL decoding.

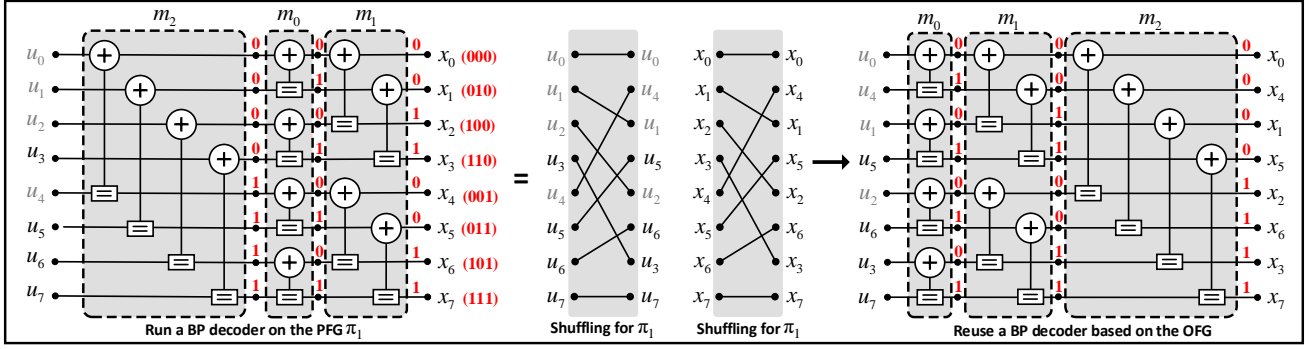


Fig. 3. Permutation of a PFG $\pi_1 = [m_2 m_0 m_1]$ based on the input shuffling.

replaces permutations of the factor graph stages.² After the above input shuffling, we use a single BP decoder based on the OFG to decode on different PFGs. Due to the varying optimal \mathcal{L} for different code configurations, it is significant for a BPL decoder to support generating the flexible input shuffling, which is discussed in Section IV.

III. PROPOSED GRAPH SELECTION ALGORITHM BASED ON THE PERMUTATION SELECTION GAIN

In this section, we derive the block error probability of serial BPL decoding and further propose the SG algorithm to obtain a near-optimal PFG set. Numerical results show that BPL decoding with the SG algorithm and $\mathbb{L} = 8$ can yield a similar performance as SCL with $\mathbb{L} = 2$ under different code rates of 5G NR polar codes. Subsequently, to fully show the potential of BP decoding, we employ the construction using the GenAlg [47] to allocate bit channels for BP decoding and apply the proposed near-optimal set. Simulations for this case illustrate that BPL decoding with $\mathbb{L} = 32$ achieves the error-correcting performance of SCL decoding with $\mathbb{L} = 4$.

A. Permutation Gain Analysis for BPL Decoding

Due to the detection module in Fig. 2, the individual block error probability $\Pr(E_l)$ for the l -th PFG $\tilde{\pi}_l$ in \mathcal{L} combines the miss rate $\Pr(M_l)$, the false-alarm rate $\Pr(F_l)$ and the error-detection rate $\Pr(D_l)$, and can be expressed as

$$\Pr(E_l) = \Pr(M_l) + \Pr(D_l) - \Pr(F_l). \quad (3)$$

Considering the serial decoding schedule, we modify the derivation for the block error probability of BPL decoding $\Pr(E_{\text{BPL}(\mathcal{L})})$ in [14], as illustrated in (4)

$$\begin{aligned} \Pr(E_{\text{BPL}(\mathcal{L})}) = & \underbrace{\sum_{l=1}^{\mathbb{L}-1} \Pr\left(M_l \mid \bigcap_{k=0}^{l-1} D_k\right)}_{\text{miss probability}} + \Pr(M_0) \\ & + \underbrace{\Pr\left(\bigcap_{l=0}^{\mathbb{L}-1} D_l\right)}_{\text{list error probability}} - \underbrace{\Pr\left(F_{\mathbb{L}-1} \mid \bigcap_{l=0}^{\mathbb{L}-2} D_l\right)}_{\text{false-alarm probability}}, \end{aligned} \quad (4)$$

where the list error probability $\Pr\left(\bigcap_{l=0}^{\mathbb{L}-1} D_l\right)$ reveals the improvement in the error-correcting performance from list

²Note that we shuffle the input LLRs R_0 and L_n in a BP decoder. For simplicity, we shuffle \mathbf{u} and \mathbf{x} in Fig. 3 to express how the shuffling works.

decoding. From (4) we also see that the probability of this term $\Pr\left(\bigcap_{l=0}^{\mathbb{L}-1} D_l\right)$ decreases as the number of PFG candidates \mathbb{L} increases. If $\mathbb{L} = 1$, $\Pr(E_{\text{BPL}(\mathcal{L})}) = \Pr(M_0) + \Pr(D_0) - \Pr(F_0)$. In serial BPL decoding, the detection module performs the CRC detection [51] instead of calculating the minimum Euclidean distance as in parallel BPL decoding [11]. Note that the CRC detection makes the output codeword not necessarily maximum-likelihood decodable and it introduces the miss probability and false-alarm probability in (4).

Most PFG selection algorithms in [15]–[17], [40] are only concerned with an efficient metric to select PFGs with the minimum $\Pr(D_l)$, $\tilde{\pi}_l \in \mathcal{L}$. However, as shown in (4), the list error probability is determined by the joint block error probability of the selected PFGs instead of the independent $\Pr(D_l)$ of each selected PFG. Therefore, the task of finding the optimal \mathcal{L}^* that yields the lowest block error probability $\Pr(E_{\text{BPL}(\mathcal{L})})$ has transformed into an optimization problem to minimize (4), as shown in (5)

$$\mathcal{L}^* = \arg \min_{\mathcal{L}} \Pr(E_{\text{BPL}(\mathcal{L})}), \text{ s.t. } |\mathcal{L}| = \mathbb{L}. \quad (5)$$

It is noteworthy that $\Pr(M_l)$ and $\Pr(F_l)$ of (4) are constants only decided by the CRC polynomial and are independent of the PFG index l . We therefore denote them as \Pr_M and \Pr_F , respectively, in the following. To simplify the optimization problem in (5), as mentioned in Section II.C, we empirically default $\tilde{\pi}_0 = \pi_0$ since the OFG always yields the lowest block error probability. Then, we reformulate (4) based on probabilities that are conditioned on $\Pr(D_0)$ to reflect the PFG selection gain

$$\begin{aligned} \Pr(E_{\text{BPL}(\mathcal{L})}) = & \Pr(D_0) \cdot \left[\Pr_M \cdot \sum_{l=2}^{\mathbb{L}-1} \Pr\left(\bigcap_{k=1}^{l-1} D_k \mid D_0\right) + \Pr_M \right. \\ & \left. + \underbrace{\Pr\left(\bigcap_{l=1}^{\mathbb{L}-1} D_l \mid D_0\right)}_{\text{PFG selection gain}} - \Pr_F \cdot \Pr\left(\bigcap_{l=1}^{\mathbb{L}-2} D_l \mid D_0\right) \right] + \Pr_M. \end{aligned} \quad (6)$$

Subsequently, we use $\mathcal{L}' = \mathcal{L} \setminus \pi_0$ to denote the remaining PFG set. In the CRC detection, \Pr_F is relatively small [51], so we further simplify (5) into (7) based on (6), in which we

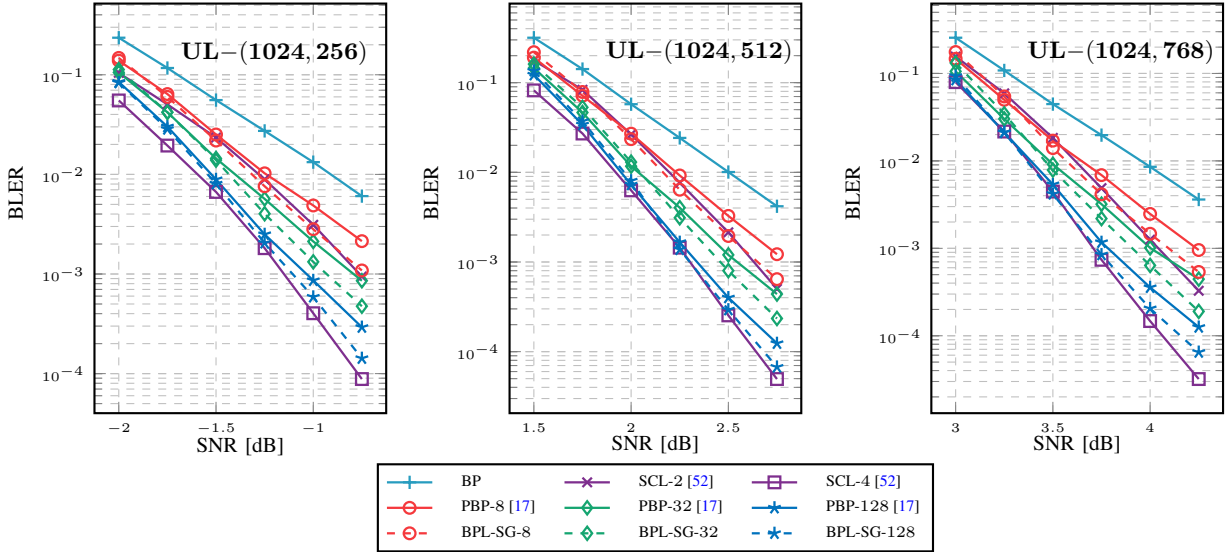


Fig. 4. BLER performance of BP, PBP, the proposed BPL-SG, and SCL decoding for 5G UL polar codes with $R = \{\frac{1}{4}, \frac{1}{2}, \frac{3}{4}\}$, respectively. All iterative decoders use CRC for detection and $I_{\max} = 50$.

eliminate the negligible term of false-alarm probability

$$\mathcal{L}^* \approx \arg \min_{\mathcal{L}'} \Pr(E_{\text{BPL}(\mathcal{L})} | D_0) \approx \arg \min_{\mathcal{L}'} \left[\underbrace{\Pr_M \cdot \sum_{l=2}^{\mathbb{L}-1} \Pr\left(\bigcap_{k=1}^{l-1} D_k | D_0\right)}_{\text{miss probability: } \Pr_{M(\mathcal{L}')}} + \underbrace{\Pr\left(\bigcap_{l=1}^{\mathbb{L}-1} D_l | D_0\right)}_{\text{PFG gain: } \Pr_{\text{PFG}(\mathcal{L}')}} \right], \quad (7)$$

where $\Pr_{M(\mathcal{L}')}$ is a constant \Pr_M when $\mathbb{L} = 2$. In order to obtain the optimal \mathcal{L}' that minimizes (7), we factorize $\Pr_{M(\mathcal{L}')}$ and $\Pr_{\text{PFG}(\mathcal{L}')}$ as shown in (8)

$$\begin{cases} \Pr_{M(\mathcal{L}')} = \Pr_M \cdot \Pr(D_1 | D_0) \cdot \left(1 + \dots \left(1 + \Pr\left(D_{\mathbb{L}-2} | \bigcap_{l=0}^{\mathbb{L}-3} D_l\right)\right)\right), \\ \Pr_{\text{PFG}(\mathcal{L}')} = \Pr(D_1 | D_0) \cdot \dots \cdot \Pr\left(D_{\mathbb{L}-1} | \bigcap_{l=0}^{\mathbb{L}-2} D_l\right), \end{cases} \quad (8)$$

where $\Pr_{M(\mathcal{L}')}$ and $\Pr_{\text{PFG}(\mathcal{L}')}$ both have a similar sequential structure. If $\mathbb{L} = 2$, (7) degenerates to $\Pr(D_1 | D_0)$ and we find $\tilde{\pi}_1$ by minimizing $\Pr(D_1 | D_0)$. When \mathbb{L} increases from 2 to 3 and we reserve the selected $\{\tilde{\pi}_0, \tilde{\pi}_1\}$, we can consecutively obtain $\tilde{\pi}_2$ by minimizing $\Pr(D_2 | D_0, D_1)$. Note that when $\mathbb{L} = 3$, $\{\tilde{\pi}_0, \tilde{\pi}_1, \tilde{\pi}_2\}$ selected by the above method is only an approximation of (7), which implies that we sequentially obtain $\tilde{\pi}_1$ and $\tilde{\pi}_2$ following a greedy algorithm.

In conclusion, through the greedy algorithm applied to the sequential structure of (8), when selecting the l -th PFG for \mathcal{L} , we always choose the $\tilde{\pi}_l$ that can minimize $\Pr(D_l | D_0, D_1, \dots, D_{l-1})$, based on the previous $l-1$ selected PFGs, $l \in [1, \mathbb{L}]$. This method decomposes the issue of minimizing the joint block error probability into $\mathbb{L} - 1$ consecutive minimization problems of conditional probabilities, which only provides a near-optimal result solution for (7).

Algorithm 1: SG Process

Input: $\mathcal{D}, \mathcal{P}, \mathbb{L}$

Output: \mathcal{L}

```
// default  $\pi_0$  is the 0-th element of  $\mathcal{L}$ 
1  $\mathcal{L}(0) \leftarrow \pi_0$ ;
2 for  $i = 0$  to  $|\mathcal{P}| - 1$  do
3   // record the failed frames as 1s
4    $\mathbf{T}(i, :) \leftarrow \text{BPEvaluate}(\mathcal{P}(i), \mathcal{D})$ ;
5   // generate the  $\mathcal{L}$ 
6   for  $l = 1$  to  $\mathbb{L} - 1$  do
7     // find the minimum  $\Pr(D_l | D_0 \dots D_{l-1})$ 
8      $i^* \leftarrow \text{selectBestList}(\mathbf{T})$ ;
9      $\mathcal{L}(l) \leftarrow \mathcal{P}(i^*)$ ;
10    // delete the corrected errors
11     $\{\mathbf{T}, \mathcal{D}\} \leftarrow \text{updateDataset}(\mathbf{T}, \mathcal{D}, i^*)$ ;
```

B. Sequential Generation (SG) Algorithm for Graph Selection

In this section, we propose a graph selection algorithm, called SG, to sequentially perform $\arg \min \Pr(D_l | D_0, D_1, \dots, D_{l-1})$ and obtain $\tilde{\pi}_l$ for \mathcal{L} , $l \in [1, \mathbb{L}]$. Additionally, due to the introduction of the conditional probability $\Pr(D_0)$ from (4) to (7), $\Pr(E_{\text{BPL}(\mathcal{L})} | D_0) \gg \Pr(E_{\text{BPL}(\mathcal{L})})$. Thus, we can use a relatively small dataset to find the remaining near-optimal $\tilde{\pi}_l$ based on Monte-Carlo simulations.

To realize the SG algorithm, we first generate a dataset \mathcal{D} , which stores $|\mathcal{D}|$ received vectors \mathbf{y} that fail to pass the CRC detection under BP decoding on π_0 . Let \mathcal{P} denote the search space of PFGs. As mentioned in Section II.C, the authors of [17] found that the PFGs which fix more left stages and only permute the right-most side of the graph tend to have a better error-correcting performance. Hence, we change p in (2) to reasonably decrease the design space of \mathcal{P} , i.e., $(n-p)!$ PFGs, and simplify computational complexity. Subsequently, for each PFG candidate, we evaluate its block error rate (BLER) performance in $\text{BPEvaluate}()$ for all received words in \mathcal{D} . The

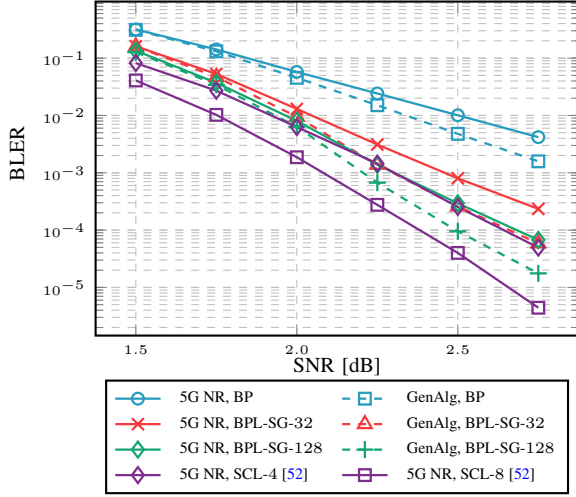


Fig. 5. BLER performance of BP, the proposed BPL-SG, and SCL decoding for (1024, 512) polar codes with GenAlg and 5G NR constructions. All iterative decoders based on OMS decoding use CRC for detection, $I_{\max} = 50$, and CRC-11 is specified by 5G NR.

current frame is recorded as ‘1’ in \mathbf{T} if failing to decode, and the matrix \mathbf{T} is dynamic with the initial dimension of $(|\mathcal{P}| \times |\mathcal{D}|)$. In Algorithm 1, the first element of \mathcal{L} is set to π_o . Then, for the i -th PFG in \mathcal{P} and the j -th received codeword in \mathcal{D} , the flag to label the success/failure of the CRC detection is marked as ‘0/1’ in $\mathbf{T}(i, j)$ depending on if decoding succeeded or not. In order to further populate \mathcal{L} , we use the function `selectBestList()` to return the index i^* that corresponds to the minimum weight row in \mathbf{T} , which is equivalent to minimizing $\Pr(D_l | D_0 \cdots D_{l-1})$. After storing $\mathcal{P}(i^*)$ into $\mathcal{L}(l)$, the function `updateDataset()` updates \mathbf{T} and \mathcal{D} by dynamically deleting the columns corresponding to the 0s in $\mathbf{T}(i^*, :)$ and corresponding samples in \mathcal{D} to only keep the erroneous cases. The above operations (lines 4 ~ 7 in Algorithm 1) are repeated for $\mathbb{L} - 1$ -times until filling \mathcal{L} .

C. Numerical Results of the Proposed Algorithm

Fig. 4 compares the BLER performance of BP decoding, permuted BP (PBP) decoding [17], SCL decoding [52], and the proposed BPL decoding with the SG algorithm (BPL-SG) for 5G UL polar codes with $N = 1024$ and $R \in \{\frac{1}{4}, \frac{1}{2}, \frac{3}{4}\}$, where all iterative decoders have the same $I_{\max} = 50$. In all following captions, the tailored “ \mathbb{L} ” denotes the employed list size. We generate a relatively small dataset \mathcal{D} with 10^6 samples that fail to pass the CRC detection under BP decoding on π_o . Note that these received vectors \mathbf{y} are collected at $\text{SNR} \in \{-1.0, 2.5, 5.5\}$ dB for $R \in \{\frac{1}{4}, \frac{1}{2}, \frac{3}{4}\}$, respectively. However, since length-1024 polar codes contain $10!$ PFGs, it is impractical to simulate all of them. In order to make a reasonable trade-off between computational complexity and performance, we set $p = 4$ in (2) and fix the left stages as $[m_0 m_1 m_2 m_3]$ to reduce the cardinality of \mathcal{P} , which now contains only 720 PFG candidates. Numerical results from simulating over AWGN channels with binary phase-shift keying (BPSK) modulation show that BPL-SG-32 provides a 0.1 dB improvement in comparison with PBP-32 at $\text{BLER} = 10^{-3}$, and this improvement increases to 0.2 dB for $R = \{\frac{1}{4}, \frac{3}{4}\}$. When \mathbb{L} increases to 128, BPL-SG further approaches the

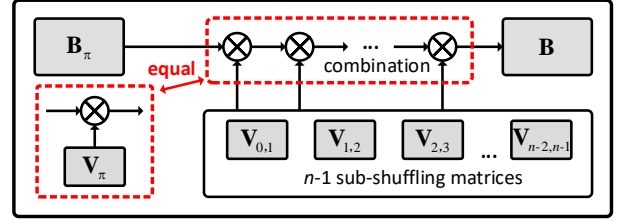


Fig. 6. Model for permutations and the generation process of the shuffling matrix \mathbf{V}_π for any PFG π .

performance of SCL-4.

In addition to the 5G NR code construction that is unfriendly to BP decoding, we also consider the GenAlg construction [47] to fully show the potential of BP decoding. Fig. 5 illustrates the BLER performance of BP, SCL, and BPL-SG decoding for (1024, 512) polar codes with the GenAlg and 5G NR constructions, in which the CRC-11 polynomial is adopted from the 5G NR standard. BPL-SG-32 under the GenAlg construction approaches the performance of SCL-4, and BPL-SG-128 under the GenAlg construction surpasses SCL-4 by 0.2 dB at $\text{BLER} = 10^{-4}$.

IV. PROPOSED ALGORITHM OF FORMULA-BASED PERMUTATION GENERATION

As mentioned in Section II.D, permutations of the factor graph stages can also be substituted efficiently by only shuffling the input LLRs to avoid instantiating multiple BP decoders with different factor graph architectures. Hence, this solution greatly facilitates the hardware implementation. However, since a variety of shuffling patterns need to be generated to realize a single shuffling set \mathcal{L} and since different code configurations require different shuffling sets, the implementation of the corresponding flexible LLR routing is the most challenging issue. In this section, we propose a hardware-friendly algorithm to generate these flexible routings, i.e., permutations. We prove that the routing of any PFG can be decomposed into a combination of $n-1$ fixed sub-routings, as shown in Fig. 6. The complicated hardware routing issue can therefore be optimized as a matrix decomposition.

A. Mathematical Model for Permutations

First, we create a model for permutations to solve the hardware routing problems with a matrix decomposition. For length- N polar codes, if the nodes \oplus and \boxminus in PFGs are represented by ‘0’ and ‘1’ respectively, any PFG can be mapped into a unique $N \times n$ binary matrix, in which the ‘0/1’ sequence in each row corresponds to the binary expansion of the bit-index for the input LLRs. For example, we use $\mathbf{B} = [b_{n-1} b_{n-2} \cdots b_1 b_0]$ to denote the OFG of Fig. 1 (contrary to its stage order $[0 \ 1 \ 2 \ \cdots \ n-1]$), and b_i is a length- N binary column vector expanded as

$$\mathbf{b}_i = \left[\underbrace{\mathbf{0}}_{1 \times 2^i} \underbrace{\mathbf{1}}_{1 \times 2^i} \mathbf{0} \mathbf{1} \cdots \mathbf{0} \mathbf{1} \right]^T, \quad i \in [0, n), \quad (9)$$

2^{n-i-1} pairs of [0 1]

where each $\mathbf{0}$ or $\mathbf{1}$ is an all-0 or all-1 row vector of length- 2^i . For any PFG π , the corresponding binary matrix \mathbf{B}_π can be written as $\mathbf{B}_\pi = [b_{\pi n-1} b_{\pi n-2} \cdots b_{\pi 1} b_{\pi 0}]$, and (10) shows

the examples of π_0 and π_1 of Fig. 1 and Fig. 3.

$$\mathbf{B} = \begin{bmatrix} 0 & 0 & 0 \\ 0 & 0 & 1 \\ 0 & 1 & 0 \\ 0 & 1 & 1 \\ 1 & 0 & 0 \\ 1 & 0 & 1 \\ 1 & 1 & 0 \\ 1 & 1 & 1 \end{bmatrix}, \quad \mathbf{B}_{\pi_1} = \begin{bmatrix} 0 & 0 & 0 \\ 0 & 1 & 0 \\ 1 & 0 & 0 \\ 1 & 1 & 0 \\ 0 & 0 & 1 \\ 0 & 1 & 1 \\ 1 & 0 & 1 \\ 1 & 1 & 1 \end{bmatrix}. \quad (10)$$

Consequently, the model for permutations based on the input shuffling can be derived as follows

$$\mathbf{B}_{\pi}^{\mathbf{T}} \cdot \mathbf{V}_{\pi} = \mathbf{B}^{\mathbf{T}} \rightarrow \begin{cases} \mathbf{b}_{\pi^{n-1}}^{\mathbf{T}} \cdot \mathbf{V}_{\pi} = \mathbf{b}_{n-1}^{\mathbf{T}}, \\ \vdots \\ \mathbf{b}_{\pi^1}^{\mathbf{T}} \cdot \mathbf{V}_{\pi} = \mathbf{b}_1^{\mathbf{T}}, \\ \mathbf{b}_{\pi^0}^{\mathbf{T}} \cdot \mathbf{V}_{\pi} = \mathbf{b}_0^{\mathbf{T}}, \end{cases} \quad (11)$$

where \mathbf{V}_{π} is the shuffling matrix to represent the targeted routing in hardware. Namely, as shown in Fig. 6, \mathbf{B}_{π} can be multiplied by the corresponding \mathbf{V}_{π} to obtain \mathbf{B} . Hence, the above problem has been modelled as how to use a unified mathematical formula to express \mathbf{V}_{π} .

B. Decomposition and Properties of \mathbf{V}_{π}

Theorem 1. For any PFG π , the shuffling matrix \mathbf{V}_{π} which satisfies $\mathbf{B}_{\pi}^{\mathbf{T}} \cdot \mathbf{V}_{\pi} = \mathbf{B}^{\mathbf{T}}$ can be decomposed into a combination of $n - 1$ fixed sub-shuffling matrices $\mathbf{V}_{i-1,i}$, $i \in [1, n)$ for length- N polar codes.

First, we provide the explicit expression for $n - 1$ sub-shuffling matrices $\mathbf{V}_{i-1,i}$, $i \in [1, n)$ for length- N polar codes

$$\begin{aligned} \mathbf{b}^{\mathbf{T}} \cdot \mathbf{V}_{i-1,i} &= \underbrace{\left[\mathbf{b}_0^{\mathbf{T}}, \mathbf{b}_{2^i}^{\mathbf{T}}, \mathbf{b}_{2^{i+1}}^{\mathbf{T}}, \dots \right]}_{2^{i+1} \text{ groups}}, \quad (12) \\ &= \underbrace{\left[\mathbf{b}_0^{\mathbf{T}}, \mathbf{b}_{2^i}^{\mathbf{T}}, \mathbf{b}_{2^{i+1}}^{\mathbf{T}}, \dots \right]}_{2^{i+1} \text{ groups}}, \end{aligned}$$

where $\mathbf{V}_{i-1,i}$ divides the input \mathbf{b} into 2^{n-i-1} groups of equal length 2^{i+1} and shuffles based on 4 sub-vectors within each group. For an intuitive understanding of Theorem 1, we use Fig. 7 to illustrate a straightforward example of length-16 polar codes, which comprises 3 sub-shuffling matrices $\{\mathbf{V}_{0,1}, \mathbf{V}_{1,2}, \mathbf{V}_{2,3}\}$ and 4 binary column vectors $\{\mathbf{b}_0, \mathbf{b}_1, \mathbf{b}_2, \mathbf{b}_3\}$ corresponding to (9) and (12). Each sub-shuffling matrix describes a unique sub-routing in hardware. Note that, due to the recursive construction of polar codes, $n - 1$ sub-routings for length- N polar codes can be decomposed into two independent copies of $n - 2$ sub-routings for length- $\frac{N}{2}$ polar codes, as shown in Fig. 7. Before the proof of Theorem 1, it is useful to introduce additional lemmas.

Lemma 1. $\forall i \in [1, n)$, $\mathbf{V}_{i-1,i}$ is an involutory matrix, i.e., $\mathbf{V}_{i-1,i} = \mathbf{V}_{i,i-1}$, $\mathbf{V}_{i-1,i} \cdot \mathbf{V}_{i,i-1} = \mathbf{I}_N$.

Based on the features of (12), the proof is straightforward. Then, we can further derive (13) as implied in Fig. 7

$$\begin{cases} \mathbf{b}_{i-1}^{\mathbf{T}} \cdot \mathbf{V}_{i-1,i} = \mathbf{b}_i^{\mathbf{T}}, \\ \mathbf{b}_i^{\mathbf{T}} \cdot \mathbf{V}_{i,i-1} = \mathbf{b}_{i-1}^{\mathbf{T}}, \end{cases} \quad \forall i \in [1, n). \quad (13)$$

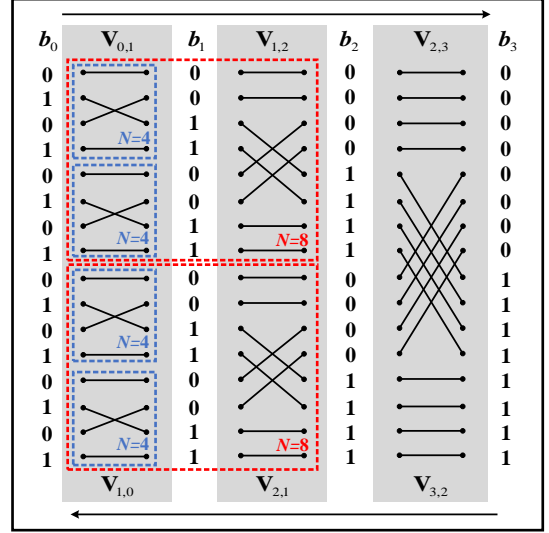


Fig. 7. Sub-shuffling matrices and binary column vectors for length-16 codes.

Lemma 2.

$$\mathbf{b}_i^{\mathbf{T}} \cdot \mathbf{V}_{i,j} = \mathbf{b}_j^{\mathbf{T}}, \quad \forall i, j \in [0, n). \quad (14)$$

Proof. We define $\mathbf{V}_{i,j} = \mathbf{V}_{i,i+1} \cdot \mathbf{V}_{i+1,i+2} \cdots \mathbf{V}_{j-1,j}$, $\forall i, j \in [0, n)$, $i < j$ and let $\mathbf{V}_{i,j} = \mathbf{I}_N$, $\forall i, j \in [0, n)$, $i = j$. Based on (13), it can be verified that $\mathbf{b}_i^{\mathbf{T}} \cdot \mathbf{V}_{i,j} = \mathbf{b}_i^{\mathbf{T}} \cdot \mathbf{V}_{i,i+1} \cdot \mathbf{V}_{i+1,j} = \mathbf{b}_{i+1}^{\mathbf{T}} \cdot \mathbf{V}_{i+1,j} = \cdots = \mathbf{b}_j^{\mathbf{T}}$. For $i \geq j$, a similar proof can be formulated. \square

Lemma 3. $\forall i, j, k \in [0, n)$, $i \neq j, k \neq i$, (15) holds.

$$\mathbf{b}_k^{\mathbf{T}} \cdot \mathbf{V}_{i,j} = \begin{cases} \mathbf{b}_k^{\mathbf{T}}, & \text{if } k \notin [\min(i, j), \max(i, j)], \\ \mathbf{b}_{k+\text{sgn}(i-j)}^{\mathbf{T}}, & \text{if } k \in [\min(i, j), \max(i, j)]. \end{cases} \quad (15)$$

An intuitive example for Lemma 3 is visible from Fig. 7: Using Lemma 2, when calculating $\mathbf{b}_3^{\mathbf{T}} \cdot \mathbf{V}_{0,2} \stackrel{2}{=} \mathbf{b}_3^{\mathbf{T}} \cdot \mathbf{V}_{0,1} \cdot \mathbf{V}_{1,2}$, we can simply permute $\mathbf{b}_3^{\mathbf{T}} = [0 \cdots 0 \ 1 \cdots 1]^{\mathbf{T}}$ through $\mathbf{V}_{0,1}$ and $\mathbf{V}_{1,2}$ and find the result still equals to $\mathbf{b}_3^{\mathbf{T}}$ since $3 \notin [0, 2]$. Besides, using Lemma 1 and 2, $\mathbf{b}_1^{\mathbf{T}} \cdot \mathbf{V}_{0,2} \stackrel{2}{=} \mathbf{b}_1^{\mathbf{T}} \cdot \mathbf{V}_{0,1} \cdot \mathbf{V}_{1,2} \stackrel{1,2}{=} \mathbf{b}_0^{\mathbf{T}} \cdot \mathbf{V}_{1,2} = \mathbf{b}_0^{\mathbf{T}}$ since $1 \in [0, 2]$ and $\text{sgn}(0 - 2) = -1$.

Proof. If $k \notin [\min(i, j), \max(i, j)]$, Lemma 3 can be verified by Lemma 1, (9), and (12). If $k \in [\min(i, j), \max(i, j)]$, we need to distinguish two cases: for $i < j$, $\mathbf{b}_k^{\mathbf{T}} \cdot \mathbf{V}_{i,j}$ can be represented by (16) and therefore

$$\begin{aligned} \mathbf{b}_k^{\mathbf{T}} \cdot \mathbf{V}_{i,j} &= \mathbf{b}_k^{\mathbf{T}} \cdot \mathbf{V}_{i,i+1} \cdots \mathbf{V}_{k-1,k} \cdot \mathbf{V}_{k,k+1} \cdots \mathbf{V}_{j-1,j} \\ &= \mathbf{b}_{k-1}^{\mathbf{T}} \cdot \mathbf{V}_{k,k+1} \cdots \mathbf{V}_{j-1,j} = \mathbf{b}_{k-1}^{\mathbf{T}}. \end{aligned} \quad (16)$$

For $i > j$, the proof for $\mathbf{b}_k^{\mathbf{T}} \cdot \mathbf{V}_{i,j} = \mathbf{b}_{k+1}^{\mathbf{T}}$ is similar. \square

Lemma 4. For any \mathbf{B}_{π} , after the matrix multiplication by $\mathbf{V}_{i-1,i}$, $\forall i \in [1, n)$, \mathbf{B}_{π} never contains two identical columns.

Proof. $\forall i \in [1, n)$, let $i - 1 = \pi^x$, $i = \pi^y$, using Lemma 1 and Lemma 3, it is apparent that

$$\begin{aligned} \mathbf{B}_{\pi}^{\mathbf{T}} \cdot \mathbf{V}_{i-1,i} &= [\mathbf{b}_{\pi^{n-1}}^{\mathbf{T}} \cdots \mathbf{b}_{\pi^x}^{\mathbf{T}} \cdots \mathbf{b}_{\pi^y}^{\mathbf{T}} \cdots \mathbf{b}_{\pi^0}^{\mathbf{T}}] \cdot \mathbf{V}_{i-1,i} \\ &\stackrel{1,3}{=} [\mathbf{b}_{\pi^{n-1}}^{\mathbf{T}} \cdots \mathbf{b}_{\pi^x}^{\mathbf{T}} \cdot \mathbf{V}_{i-1,i} \cdots \mathbf{b}_{\pi^y}^{\mathbf{T}} \cdot \mathbf{V}_{i-1,i} \cdots \mathbf{b}_{\pi^0}^{\mathbf{T}}] \\ &= [\mathbf{b}_{\pi^{n-1}}^{\mathbf{T}} \cdots \mathbf{b}_{\pi^y}^{\mathbf{T}} \cdots \mathbf{b}_{\pi^x}^{\mathbf{T}} \cdots \mathbf{b}_{\pi^0}^{\mathbf{T}}]. \end{aligned} \quad (17)$$

Hence, for any π , the matrix multiplication by any $\mathbf{V}_{i-1,i}, i \in [1, n)$ is equivalent to swapping two columns of \mathbf{B}_π . \square

Lemma 5. For any \mathbf{B}_π , if executing a right-to-left column-wise transformation to realize $\mathbf{B}_\pi \rightarrow \mathbf{B}$, the previously matched columns are never influenced by the current shuffling matrix.

Proof. $\forall i \in [0, n]$, there are i matched columns on the right and $n - i$ un-matched columns on the left of \mathbf{B}_π compared with \mathbf{B} , as shown in (18)

$$\begin{aligned} \mathbf{B}_{\pi_{s_i}} &= \underbrace{[\mathbf{b}_{\pi_{s_i}^{n-1}} \dots \mathbf{b}_{\pi_{s_i}^i}]}_{\text{un-matched}} \underbrace{[\mathbf{b}_{i-1} \dots \mathbf{b}_0]}_{\text{matched}} \\ &\rightarrow \mathbf{B} = [\mathbf{b}_{n-1} \dots \mathbf{b}_i \mathbf{b}_{i-1} \dots \mathbf{b}_0], \end{aligned} \quad (18)$$

where π_{s_i} denotes the original π after i transformations. Subsequently, we multiply the shuffling matrix $\mathbf{V}_{\pi_{s_i}^i, i}$ to obtain (19)

$$\begin{aligned} &\underbrace{[\mathbf{b}_{\pi_{s_i}^{n-1}} \dots \mathbf{b}_{\pi_{s_i}^i}]}_{\text{un-matched}} \underbrace{[\mathbf{b}_{i-1} \dots \mathbf{b}_0]}_{\text{matched}} \cdot \mathbf{V}_{\pi_{s_i}^i, i} \\ &= \underbrace{[\{\mathbf{b}_{\pi_{s_i}^{n-1}} \dots \mathbf{b}_{\pi_{s_i}^i}\}]}_{\text{un-matched}} \cdot \mathbf{V}_{\pi_{s_i}^i, i} \underbrace{[\mathbf{b}_{i-1} \dots \mathbf{b}_0]}_{\text{matched}} \cdot \mathbf{V}_{\pi_{s_i}^i, i} \\ &= \underbrace{[\mathbf{b}_{\pi_{s_i+1}^{n-1}} \dots \mathbf{b}_{\pi_{s_i+1}^{i+1}}]}_{\text{un-matched}} \underbrace{[\mathbf{b}_i^T \mathbf{b}_{i-1}^T \dots \mathbf{b}_0^T]}_{\text{matched}}. \end{aligned} \quad (19)$$

In accordance with Lemma 4, the un-matched columns in \mathbf{B}_π never contain any element of $[\mathbf{b}_{i-1}^T \dots \mathbf{b}_0^T]$. Therefore, we can derive that $\pi_{s_i}^i > i - 1$ and $[\mathbf{b}_{i-1}^T \dots \mathbf{b}_0^T] \cdot \mathbf{V}_{\pi_{s_i}^i, i} \stackrel{3}{=} [\mathbf{b}_{i-1}^T \dots \mathbf{b}_0^T]$ always holds. Besides, combined with Lemma 1, we further obtain $\mathbf{b}_{\pi_{s_i}^i}^T \cdot \mathbf{V}_{\pi_{s_i}^i, i} = \mathbf{b}_i^T$ and let $\pi_{s_{i+1}}$ denote the original π after $i + 1$ transformations. Hence, the proof of Lemma 5 has been completed. \square

In conclusion, combined with the aforementioned Lemma 1-5, the proof of Theorem 1 is provided below.

Proof of Theorem 1. The decomposition process of any permutation is illustrated in (20), which clearly presents how to generate the shuffling matrix \mathbf{V}_π .

$$\begin{aligned} \mathbf{B}_\pi^T \cdot \mathbf{V}_{\pi^0, 0} &= \mathbf{B}_{\pi_{s_1}}^T = [\mathbf{b}_{\pi_{s_1}^{n-1}}^T \dots \mathbf{b}_{\pi_{s_1}^1}^T \mathbf{b}_0^T], \\ \mathbf{B}_{\pi_{s_1}}^T \cdot \mathbf{V}_{\pi_{s_1}^1, 1} &= \mathbf{B}_{\pi_{s_2}}^T = [\mathbf{b}_{\pi_{s_2}^{n-1}}^T \dots \mathbf{b}_{\pi_{s_2}^2}^T \mathbf{b}_1^T \mathbf{b}_0^T], \\ &\dots \\ \mathbf{B}_{\pi_{s_{n-1}}}^T \cdot \mathbf{V}_{\pi_{s_{n-1}}^{n-1}, n-1} &= \mathbf{B}^T = [\mathbf{b}_{n-1}^T \dots \mathbf{b}_1^T \mathbf{b}_0^T], \end{aligned} \quad (20)$$

where we rewrite π^0 as $\pi_{s_0}^0$ to obtain a unified mathematical notation and further simplify the process of (20) by (21)

$$\begin{aligned} \mathbf{B}_\pi^T \cdot \mathbf{V}_\pi &= \mathbf{B}_\pi^T \cdot \mathbf{V}_{\pi_{s_0}^0, 0} \cdot \mathbf{V}_{\pi_{s_1}^1, 1} \dots \mathbf{V}_{\pi_{s_{n-1}}^{n-1}, n-1} \\ &= \mathbf{B}_\pi^T \cdot \prod_{i=0}^{n-1} \mathbf{V}_{\pi_{s_i}^i, i}, \end{aligned} \quad (21)$$

in which we obtain the final expression for \mathbf{V}_π as

$$\mathbf{V}_\pi = \prod_{i=0}^{n-1} \mathbf{V}_{\pi_{s_i}^i, i}, \quad (22)$$

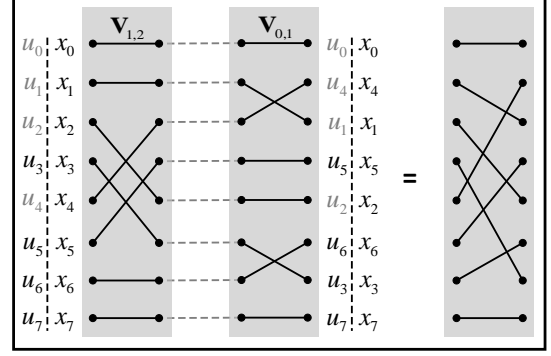


Fig. 8. Shuffling the input LLRs based on a matrix decomposition for $\pi_1 = [m_2 \ m_0 \ m_1]$.

Algorithm 2: Generation of Permutations by A Matrix Decomposition

Input: \mathbf{R}_0 , PFG = $[\pi^0 \ \pi^1 \ \dots \ \pi^{n-1}]$, and OFG = $[0 \ 1 \ \dots \ n - 1]$

Output: \mathbf{R}_0

// initialization

1 $\mathbf{s} \leftarrow \{\mathbf{0}\}$; // store $\pi_{s_0}^0, \pi_{s_1}^1, \dots, \pi_{s_{n-1}}^{n-1}$
// $n - 1$ sub-shuffling matrices

2 $\mathbf{V}_{\text{set}} = [\mathbf{V}_{0,1} \ \mathbf{V}_{1,2} \ \dots \ \mathbf{V}_{n-2,n-1}]$;
// generate \mathbf{V}_π

3 **for** $i = 0$ to $n - 1$ **do**

4 $s = \text{PFG}[i]$; // current column $\pi_{s_i}^i$

5 $e = \text{OFG}[i]$; // aimed column i
// update PFG by $\mathbf{V}_{s,e}$

6 **for** $j = i$ to $n - 1$ **do**

7 $\text{PFG}[j] \leftarrow \text{updateStage}(\text{PFG}[j], s, e)$;

8 $\mathbf{s}[i] = s$; // store the current $\pi_{s_i}^i$

// execute \mathbf{V}_π to permute input LLRs

9 **for** $i = 0$ to $n - 1$ **do**

10 $\mathbf{R}_0 \leftarrow \text{subRouting}(\mathbf{R}_0, \mathbf{V}_{\text{set}}, \mathbf{s}[i], \text{OFG}[i])$;

where $\mathbf{V}_{\pi_{s_i}^i, i}$ can be expressed as a product from $n - 1$ sub-shuffling matrices $\mathbf{V}_{i-1,i}, i \in [1, n)$, based on Lemma 2. \square

C. A Hardware-Friendly Algorithm by Matrix Decomposition

Note that the derivation of \mathbf{V}_π in Section IV.B is from the perspective of the mapped binary matrix ($\mathbf{B}_\pi^T \cdot \mathbf{V}_\pi = \mathbf{B}^T$) of the factor graph to interpret how to generate \mathbf{V}_π . However, as mentioned in Section II.D, the effect of \mathbf{V}_π is to shuffle the input LLRs into a specific order in a practical decoder. An intuitive example is shown in Fig. 8: For $\pi_1 = [m_2 \ m_0 \ m_1]$ of length-8 polar codes, we generate $\mathbf{V}_{\pi_1} = \mathbf{V}_{1,2} \cdot \mathbf{V}_{0,1}$, based on (22). Then, we can permute \mathbf{u} and \mathbf{x} through two routings corresponding to $\mathbf{V}_{1,2}$ and $\mathbf{V}_{0,1}$, which is equivalent to instantiating the routing of Fig. 3. Herein, the generation of \mathbf{V}_π and the process of shuffling the input LLRs are summarized in Algorithm 2.

First, \mathbf{V}_{set} is initialized with $n - 1$ sub-shuffling matrices $\mathbf{V}_{i-1,i}, i \in [1, n)$, which are defined in (12). Note that the vector \mathbf{s} stores the sequences of sub-shuffling indices that generate $\pi_{s_i}^i$ as in (22) and are found during the decomposition

Algorithm 3: updateStage ()

Input: π^{in}, s, e
Output: π^{out}

- 1 **if** $\pi^{\text{in}} == s$ **then**
- 2 $\pi^{\text{out}} = e$; // Lemma 2
- 3 **else if** $\pi^{\text{in}} \in [\min(s, e), \max(s, e)]$ and $s \neq e$ **then**
- 4 $\pi^{\text{out}} = \pi^{\text{in}} + \text{sgn}(s - e)$; // Lemma 3
- 5 **else**
- 6 $\pi^{\text{out}} = \pi^{\text{in}}$; // keeps constant

Algorithm 4: subRouting ()

Input: $R_0, \mathbf{V}_{\text{set}}, s, e$
Output: \mathbf{V}_π

- 1 **if** $s < e$ **then**
- 2 **for** $i = s; i \leq e - 1; i++$ **do**
- 3 $R_0^T = R_0^T \cdot \mathbf{V}_{\text{set}}[i]$;
- 4 **else if** $s > e$ **then**
- 5 **for** $i = s - 1; i \geq e; i--$ **do**
- 6 $R_0^T = R_0^T \cdot \mathbf{V}_{\text{set}}[i]$;

of the shuffling. There are two main phases in Algorithm 2: generate \mathbf{V}_π and execute \mathbf{V}_π . To fill s , we run a for loop in lines 4 – 9 of Algorithm 2 to perform the right-to-left column-wise transformation as shown in (20). Namely, performing the i -th loop is equivalent to updating the PFG by $\mathbf{V}_{\pi_{s_i}^i, i}$ ($\mathbf{B}_{\pi_{s_i}} \rightarrow \mathbf{B}_{\pi_{s_{i+1}}}$ in (20)). As shown in Algorithm 3, updateStage() implements the functions of Lemma 2 and Lemma 3. Note that for length- N polar codes, we can fill s completely within n steps to generate \mathbf{V}_π .

Subsequently, we run subRouting() as shown in Algorithm 4 to permute the input LLRs R_0 (or L_n) based on the stored s . This function multiplies R_0 by $\mathbf{V}_{\pi_{s_i}^i, i}$ that can be decomposed into a product of $|\pi_{s_i}^i - i|$ sub-shuffling matrices. Finally, we transmit the permuted R_0 to the BP decoder based on the OFG.

V. PROPOSED BPL DECODER ARCHITECTURE

In this section, we present the architecture of our BPL decoder, which, to the best of our knowledge, is the first hardware implementation of a BPL decoder for polar codes. Fig. 9 illustrates the overall hardware architecture, which comprises a double-column bidirectional-propagation BP unit (BPU) [39], a permutation generator unit (PGU) as proposed in the previous section to generate flexible permutations, a termination and detection unit (TDU), a recovery module, and a controller.

A. Architecture Overview

For the underlying BPU, we employ the SOA double-column bidirectional-propagation architecture [39]. The dataflows of R- and L-messages are performed simultaneously, which means that R-messages at the j -th stage and L-messages at the $(n-j)$ -th stage are calculated in the same clock cycle (CC). We store the input LLRs R_0 and L_n in the memory R_0 and the memory L_n , respectively. The PGU shuffles the input LLRs according to Algorithm 2 to generate the shuffled input LLRs R'_0 and L'_n for \mathbb{L} PFGs. Same as [39], the proposed decoder reduces

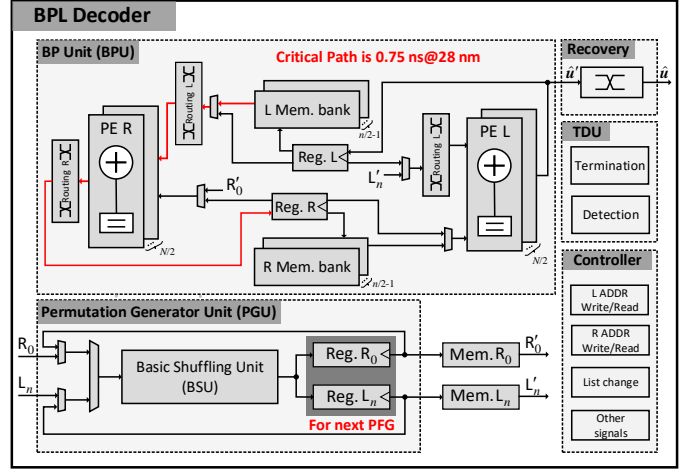


Fig. 9. Hardware architecture of our BPL decoder, where solid black lines denote data signals and solid red lines denote the critical path.

the number of CCs per internal iteration from n to $n - 1$ by removing the calculation of R_n and L_0 messages. Besides, we use a sign-assisted (SA) termination strategy [22], [53] to check the sign convergence of the internal results. The SA strategy terminates decoding when hard decisions in the BPU are identical in three consecutive iterations, as shown in the termination module on the right side of Fig. 9. Finally, a detection module performs the CRC detection to judge whether output the current decoded \hat{u} or decode on a new PFG further, which is discussed in Section V.C.

B. Permutation Generation Unit (PGU)

1) *Hardware Architecture:* Based on the shuffling matrix derived in Section IV, we implement a low-complexity permutation network PGU for the BPL decoder, which comprises a basic shuffling unit (BSU), two registers for R_0 and L_n , and some MUXes. For the BSU shown in Fig. 10, we instantiate $n - 1$ fixed sub-routings ($\mathbf{V}_{i-1, i}, i \in [1, n)$) to realize all the required basic shuffling. All the stage orders of the proposed near-optimal PFG set $\mathcal{L} (\{\tilde{\pi}_l^0, \tilde{\pi}_l^1, \dots, \tilde{\pi}_l^{n-1}\}, l \in [0, \mathbb{L})$) from the SG algorithm in Section III.B) is generated offline and stored in the PFG memory. The inputs of the BSU are the NQ -bit initial input LLRs (R_0 or L_n , and each LLR is quantized as Q bits) to be shuffled and the PFG index l of the selected PFG. First, the controller of the BSU uses n CCs to obtain the set s of Algorithm 2 based on the output from the PFG memory, i.e., the stage orders of $\tilde{\pi}_l$. Subsequently, the BSU executes Algorithm 4 step by step and controls the MUX to store the correct shuffled results into registers. Note that, in order to make a trade-off between the hardware complexity and the latency of the permutation, we only perform one sub-routing per CC to shuffle the input LLRs. For example, to realize $\mathbf{V}_{1,5}$, we decompose it as $\mathbf{V}_{1,2}, \mathbf{V}_{2,3}, \mathbf{V}_{3,4}$, and $\mathbf{V}_{4,5}$ to sequentially perform the desired permutations in 4 CCs. This decomposition process means that the latency for the permutation generation of any PFG is varying, as shown in (23),

$$\mathcal{L}_\pi = \sum_{i=0}^{n-1} |\pi_{s_i}^i - i| + n, \quad (23)$$

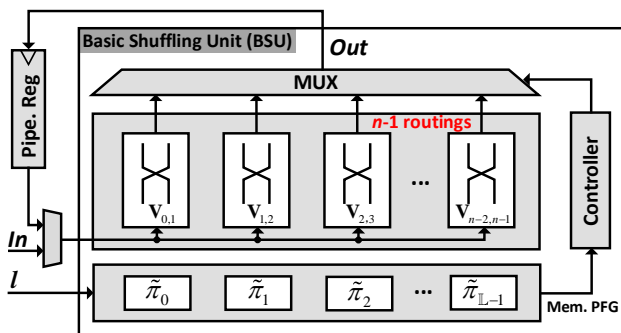


Fig. 10. The core architecture of the permutation generation unit (PGU), based on the basic shuffling unit (BSU) and outside registers.

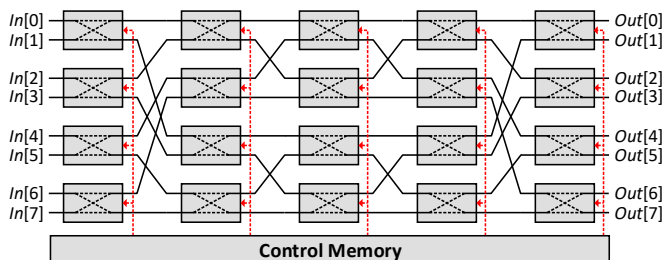


Fig. 11. Architecture of a length-8 Beneš network [41].

where $\pi_{s_i}^i$ comes from (22). The maximum latency of the BSU is $\mathcal{L}_\pi = \frac{n \cdot (n-1)}{2} + n$ CCs when the PFG is $[n-1 \ n-2 \ \dots \ 1 \ 0]$.

2) *Comparison With the Beneš Network:* To highlight the advantage of our permutation network, we reproduce the classical Beneš network [41] illustrated in Fig. 11 to make a fair comparison. The number of inputs for a regular Beneš network is a power of two ($N = 2^n$). It has $2n - 1$ stages, each with $N/2$ switches of size 2×2 . However, due to lack of an explicit method to generate control signals for PFGs in the Beneš network on the fly, for each $\tilde{\pi}_l$ in \mathcal{L} , one would need to store $\frac{N(2n-1)}{2}$ bits in the control memory to configure the ‘BAR’ or ‘CROSS’ states of each 2×2 switch, as shown in dashed red lines in Fig. 11. It is obvious to see that the area of the control memory in the Beneš network linearly grows with the maximum list size.

Synthesis results show that, for length-1024 polar codes, the area of our flexible permutation generator shown in Fig. 10 under different list sizes is only 0.076 mm². This network supports an arbitrary number of PFG candidates without any area overhead. Compared to the Beneš network³, our work has a {86.9%, 96.3%} smaller area when $\mathbb{L} \in \{8, 32\}$, respectively. In terms of the permutation latency, the average \mathcal{L}_π of all 10! PFGs is 32.5 CCs, and the maximum \mathcal{L}_π is 55 CCs, which is higher than that of the Beneš network. However, to alleviate this issue, we propose an optimized decoupled decoding schedule beneficial to the serial architecture, which is discussed in detail in Section V.D.

³The routing area of the Beneš network can be further reduced by a folded architecture to iteratively shuffle outputs, but this is beyond the scope of this paper. Moreover, the control memory occupies {75%, 89%} of the area of the Beneš network for $\mathbb{L} \in \{8, 32\}$, respectively.

TABLE I
SYNTHESIS RESULTS OF DIFFERENT PERMUTATION NETWORKS FOR LENGTH-1024 POLAR CODES IN 28NM FD-SOI WITH A 0.75NS TARGET

List	This work		Beneš work [41] [†]	
	8	32	8	32
Area [mm ²]	0.076		0.579	2.055
Avg latency [CC]	32.5		1	
Max latency [CC]	55			

[†] [41] was re-implemented and synthesized in 28 nm FD-SOI.

C. Termination and Detection Module (TDU)

The TDU is integrated into the decoder and responsible for terminating the decoding once it has converged and for performing the CRC detection between BP decoding. As described in Section V.A, we adopt the SA strategy [22], [53] to terminate the decoding if the hard decisions in the BPU are identical in three consecutive iterations. Subsequently, if passing the termination module in Fig. 9 or achieving I_{\max} (as the green SA shows in Fig. 12), the BPL decoder requires 1 CC to calculate the final HD results \hat{u}' . Since the decoded codeword \hat{u}' is permuted, to perform the CRC detection, we transform \hat{u}' to \hat{u} with the natural order in the recovery module. Note that this transformation is only the inverse process of the permutation generation in Section V.B, but the bit-width of this permutation network is only N -bit instead of NQ -bit. The latency of recovering \hat{u} is $(\mathcal{L}_\pi - n)$ CCs. If the CRC detection succeeds, \hat{u} is output from our BPL decoder.

D. Optimized Decoding Schedule

To improve the throughput of the BPL decoder, we need to avoid the influence of the latency from the proposed permutation network. To this end, we propose an optimized decoding schedule which decouples the BPU, PGU, and the recovery modules with pipeline registers to allow them to work in parallel. First, when the BPU works on $\tilde{\pi}_l, l \in [0, \mathbb{L} - 1]$, the PGU is activated to shuffle the input LLRs for the next PFG $\tilde{\pi}_{l+1}$. Since there are two kinds of the input LLRs in BP decoding (R_0 and L_n). We use the module in Fig. 10 to shuffle R_0 and L_n one after another in the same hardware. The detailed timing schedule of the proposed BPL decoder is illustrated in Fig. 12. To distinguish the shuffled input LLRs for different PFGs, we denote $R_{0, \tilde{\pi}_l}$ and $L_{n, \tilde{\pi}_l}$ as the permuted input signals R'_0 and L'_n for $\tilde{\pi}_l$. When the BPL decoder performs BP decoding on $\tilde{\pi}_l, l \in [0, \mathbb{L} - 1]$, after the PGU has already generated $R_{0, \tilde{\pi}_{l+1}}$ and $L_{n, \tilde{\pi}_{l+1}}$, these two signals are temporarily stored into the register R_0 and the register L_n that are marked with a dark grey background in Fig. 9. Once BP decoding on $\tilde{\pi}_l$ passes the termination module, the memory R_0 and the memory L_n are updated by the register R_0 and the register L_n to output $R_{0, \tilde{\pi}_{l+1}}$ and $L_{n, \tilde{\pi}_{l+1}}$ as R'_0 and L'_n for the next BP decoding on $\tilde{\pi}_{l+1}$.

Moreover, as said in Section V.C, the recovery from \hat{u}' to \hat{u} also harms the throughput of the BPL decoder, since the inverse permutation operations come at the cost of $\mathcal{L}_\pi - n$ CCs. To deal with this issue, we further decouple the recovery module from the decoding schedule. This decoupled decoding schedule allows the BPU, the PGU, and the recovery modules to work on $\{\tilde{\pi}_{l+1}, \tilde{\pi}_l, \tilde{\pi}_{l-1}\}, l \in [1, \mathbb{L} - 1]$, respectively, which

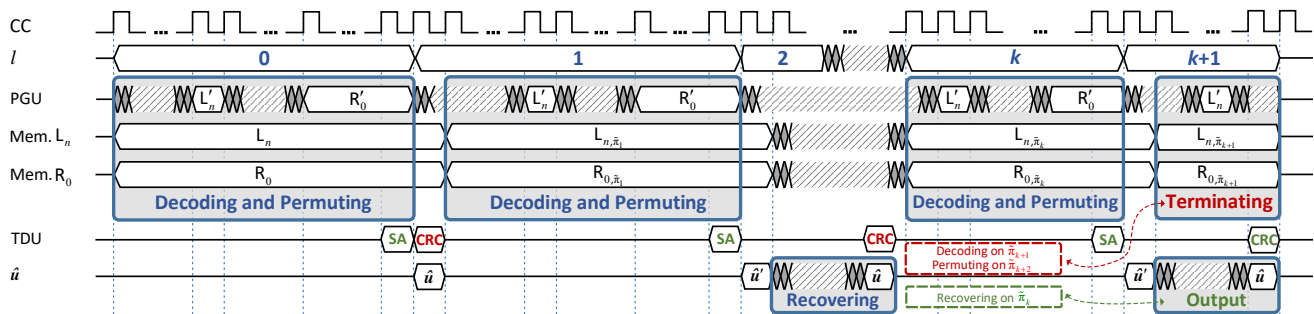


Fig. 12. Timing schedule of the proposed BPL decoder, which decodes successfully on $\tilde{\pi}_k$.

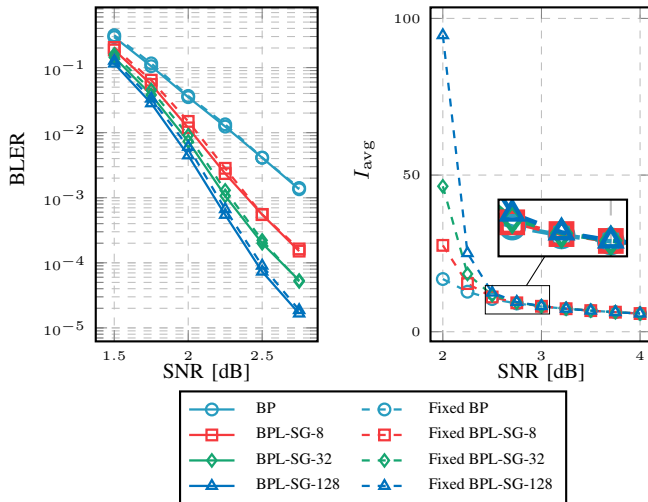


Fig. 13. BLER comparison between floating-point and fixed-point and I_{avg} of the BPL decoder equipped with the proposed near-optimal set for (1024, 512) polar codes, $\mathbb{L} \in \{8, 32, 128\}$, and $I_{\text{max}} = 50$.

significantly improves the throughput of the BPL decoder and enhances the hardware utilization. For example, we assume that the BPL decoder has successfully decoded on $\tilde{\pi}_k$ in Fig. 12. When passing the CRC detection on $\tilde{\pi}_k$, the BPL decoder terminates the decoding on $\tilde{\pi}_{k+1}$ and the permutation generation on $\tilde{\pi}_{k+2}$.

VI. IMPLEMENTATION RESULTS

In this section, we present the synthesis results for our BPL implementation. All synthesis results are based on 28 nm FD-SOI technology in the typical-typical corner, and we use timing constraints that are not achievable to maximum the operating frequency for our design. A comparison with the SOA polar decoders is also provided.

A. Quantized Performance

In Fig. 13, under the GenAlg construction, we present the BLER performance and the average number of iterations I_{avg} of our BPL decoder using floating-point and fixed-point (2's complement). Let $Q_{q_i.q_f}$ denote a fixed-point number with one sign-bit, $q_i - q_f - 1$ integer bits, and q_f fractional bits. We adopt $Q_{7.2}$ for the LLRs in Fig. 13. Numerical results show that $Q_{7.2}$ almost approaches the floating-point performance of OMS polar decoding with $[\beta_R \ \beta_L] = [0.25 \ 0]$ providing a well-balanced trade-off between the error-correcting performance and hardware complexity. For the I_{avg} of our BPL decoder,

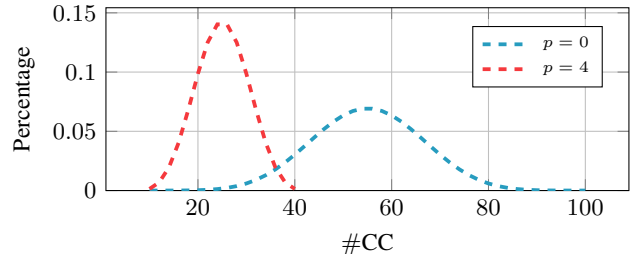


Fig. 14. Latency distribution for permuting R_0 or L_n of all PFGs for length-1024 polar codes, based on the proposed permutation network.

the influence of the list size is mainly reflected in the low SNR regions, which achieves 47.8 and 98.5 iterations for $\mathbb{L} \in \{32, 128\}$ at SNR = 2.0 dB, respectively. However, as SNR increases, the I_{avg} of the BPL decoder converges rapidly to that of the BP decoder, which achieves $I_{\text{avg}} = 5.81$ for $\mathbb{L} \in \{32, 128\}$.

B. Latency Analysis

Fig. 14 shows the latency distribution for permuting R_0 and L_n of all PFGs for length-1024 polar codes (i.e., $p = 0$) based on the PGU. For any PFG, the latency of the PGU is denoted by \mathcal{L}'_{π} in (24)

$$\mathcal{L}'_{\pi} = 2\mathcal{L}_{\pi} - n = 2 \sum_{i=0}^{n-1} |\pi_{s_i}^i - i| + n, \quad (24)$$

where the multiplication with 2 is due to the reuse of the BSU module in Fig. 9 to shuffle R_0 and L_n . This latency distribution presents an approximately normal distribution trend: the minimum is 10 CCs and the maximum is 100 CCs. Note that, for all 10! PFGs, \mathcal{L}'_{π} of 96% PFGs is lower than 80 CCs. Subsequently, when combined with the aforementioned BPL-SG algorithm, if we set $p = 4$ in (2) (left stages fixed as $[m_0 \ m_1 \ m_2 \ m_3]$) to efficiently decrease the search space of PFGs, the dynamic range of the \mathcal{L}'_{π} distribution rapidly narrows, i.e., the maximum \mathcal{L}'_{π} has a 60% reduction from 100 CCs to 40 CCs, as shown in Fig. 14.

Consequently, the whole decoding latency of our BPL decoder is calculated by (25), where $I_{\tilde{\pi}_l}$ denotes a practical iteration number of $\tilde{\pi}_l$ and k is the index of the first PFG that delivers a successfully decoded codeword. Note that, to satisfy the uniformity of (25), we set $\mathcal{L}'_{\tilde{\pi}_l} = \emptyset$, $\mathcal{L}'_{\tilde{\pi}_{-1}} = \emptyset$, and $\mathcal{L}'_{\tilde{\pi}_0} = 0$. The max operation represents how the proposed decoupled decoding schedule alleviates the influence of the

TABLE II
COMPARISON WITH THE SOA POLAR DECODERS FOR (1024, 512) POLAR CODES

Decoders	This work	[SSCL'22] [45]	[TCAS-I'19] [39]	[TVLSI'17] [38]	[TCAS-II'20] [20]	[TCOM'20] [21]	[TSP'17] [6]	[TCAS-I'20] [54]	[TSP'22] [9]
Algorithm	BPL [†]	BP [◊]	BP	BP [◊]	EBPF	GBPF-MS	Fast-SSCL	Fast-SSCF	SR-List
Process [nm]	28	40	40	65	65	40	65	65	28
Quantization [bit]	7	6	5	5	7	6	6	6	6
List/Attempt	8 32 128	—	—	—	10	10	4	20	4
SNR@BLER = 10 ⁻⁴ §	2.85 2.65 2.5	3.75	3.9	3.75	2.75	2.80	2.65	2.96	2.65
Avg Iter./Attempt*§	5.81	4.78	6.51	4.78	4.48	4.53	—	1.01	—
Area [mm ²]	0.87	2.07	0.70	1.60	3.11	0.95	1.822	0.56	0.286
Frequency [MHz]	1333	150	500	334	319	806	840	455	1255
Worst-Case T/P§ [Gb/s]	0.37 0.09 0.02	0.16	1.12	1.37	0.03	0.08	1.61	0.076	3.62
Coded T/P*§ [Gb/s]	25.63	1.69	8.59	14.31	3.61	9.01	1.61	1.51	3.62
Normalized to 28 nm, 1.0 V [‡]									
Coded T/P*§ [Gbps]	25.63	2.42	12.27	33.22	8.37	12.87	3.73	3.51	3.62
Area Eff.*§ [Gbps/mm ²]	29.46	2.38	35.79	111.89	14.50	27.65	11.05	33.73	12.67

[‡] Normalized to 28 nm technology: area $\propto s^2$ and frequency $\propto 1/s$.

* Average number of iterations for BP and average number of attempts for SC.

[†] This work and [39] employ the double-column bidirectional-propagation architecture.

[◊] [45] adopts the dual-mode architecture for LDPC and polar codes, and [38] employs the four-column architecture.

[§] Results reported at SNR = 4.0 dB, where the quantized performance of the BP works is reproduced under the GenAlg construction and $I_{\max} = 50$, and the quantized performance of the SC works is reproduced under 5G NR construction.

permutation latency and of the recovery latency. If we keep I_{\max} relatively large, the decoding latency on $\tilde{\pi}_l$ is always dominating in the max term. Numerical results show that when $I_{\max} \geq 15$, (25) can be simplified as

$$\mathcal{L}_{\text{BPL}} \approx \sum_{l=0}^k ((n-1) \cdot I_{\tilde{\pi}_l}) + k + 1 + \mathcal{L}_{\tilde{\pi}_k} - n, \quad (26)$$

where $k \in [0, \mathbb{L})$. The average latency of our BPL decoder for (1024, 512) polar codes with $\mathbb{L} = 32$ and $I_{\max} = 50$ is only 53.25 CCs at SNR = 4 dB.

C. Comparisons With Previous Works

In Table II, we present the implementation results of the proposed BPL decoder and compare with the SOA architectures in [6], [20], [21], [38], [39], [45], [54]. For a fair comparison, we reproduce the fixed-point performance of those BP-based decoders with the GenAlg construction and $I_{\max} = 50$ and the SC-based decoders with the 5G NR constructions. Note that all the previous works are normalized to 28 nm technology. For $\mathbb{L} = 32$, our decoder with a near-optimal PFG set can achieve the error-correcting performance of BLER = 10⁻⁴ at SNR = 2.65 dB, which is similar to that of Fast-SSCL-4 in [6] and better than other BP and BPF works. In terms of implementation results, our work has no advantage in terms of worst-case throughput, which is a common problem for a serial architecture. However, our BPL decoder has an average throughput of 25.63 Gbps, which is 2.09 \times , 1.99 \times , 7.30 \times , and 7.08 \times higher than the SOA BP [39], BPF [21], SC flip (SCF) [54], and SCL decoders [9], respectively. Our throughput is 22.8% lower than [38], but we see a 1.25 dB SNR improvement when $\mathbb{L} = 128$. Compared to other advanced BP decoders, such as BPF,

the area efficiency of our work is 2.03 \times and 1.07 \times higher than that of [20] and [21], respectively. It is notable that, different from the SCL works [6], [9] that instantiate \mathbb{L} independent SC decoders, our BPL decoder reuses a single BP decoder based on a serial decoding schedule and generates flexible permutations on the fly during the real-time decoding. Therefore, even if the list size is increased, the area and operating frequency of our BPL decoder are not affected.

VII. CONCLUSION

In this paper, we present an efficient BPL decoder implementation, which supports flexible permutation generation. In terms of the algorithmic contributions, we propose a sequential generation algorithm to obtain a near-optimal PFG set. Subsequently, we propose a hardware-friendly algorithm to generate flexible routings for permutations in hardware on the fly by a matrix decomposition. On the architecture level, we present the BPL decoder with several optimizations to significantly reduce the hardware complexity and decoding latency, such as the flexible permutation generator and decoupled decoding schedule. Synthesis results show that our BPL decoder can achieve a throughput of 25.63 Gbps and an area efficiency of 29.46 Gbps/mm² at SNR = 4.0 dB, which outperforms other existing SOA BP and BPF decoders. Moreover, our BPL decoder efficiently implements the decoding on multiple PFGs and provides the inspiration for the implementation of the generalized AE decoding.

REFERENCES

- [1] E. Arıkan, "Channel polarization: A method for constructing capacity-achieving codes," *IEEE Trans. Inf. Theory*, vol. 55, no. 7, pp. 3051–3073, Jul. 2008.

$$\mathcal{L}_{\text{BPL}} = \sum_{l=0}^k \max \left(\underbrace{(n-1) \cdot I_{\tilde{\pi}_l}}_{\text{decoding on } \tilde{\pi}_l}, \underbrace{\mathcal{L}'_{\tilde{\pi}_{l+1}}}_{\text{permutation on } \tilde{\pi}_{l+1}}, \underbrace{\mathcal{L}_{\tilde{\pi}_{l-1}} - n}_{\text{recovery on } \tilde{\pi}_{l-1}} \right) + \underbrace{k+1}_{\text{calculate } \hat{\mathbf{u}}'} + \underbrace{\mathcal{L}_{\tilde{\pi}_k} - n}_{\text{recovery on } \tilde{\pi}_k}, \quad k \in [0, \mathbb{L}). \quad (25)$$

- [2] *Chairman's Notes of Agenda Item 7.1.5 Channel coding and modulation*, 3GPP TSG RAN WG1 Meeting #87 R1-1613710, Nov. 2016.
- [3] I. Tal and A. Vardy, "List decoding of polar codes," *IEEE Trans. Inf. Theory*, vol. 61, no. 5, pp. 2213–2226, Mar. 2015.
- [4] K. Niu and K. Chen, "CRC-aided decoding of polar codes," *IEEE Commun. Lett.*, vol. 16, no. 10, pp. 1668–1671, Sep. 2012.
- [5] S. A. Hashemi, C. Condo, and W. J. Gross, "A fast polar code list decoder architecture based on sphere decoding," *IEEE Trans. Circuits Syst. I*, vol. 63, no. 12, pp. 2368–2380, Dec. 2016.
- [6] S. A. Hashemi, C. Condo, and W. J. Gross, "Fast and flexible successive-cancellation list decoders for polar codes," *IEEE Trans. Signal Process.*, vol. 65, no. 21, pp. 5756–5769, Aug. 2017.
- [7] M. Hanif, M. H. Ardakani, and M. Ardakani, "Fast list decoding of polar codes: Decoders for additional nodes," in *Proc. IEEE Wireless Commun. Networking Conf. Workshops (WCNC)*, 2018, pp. 37–42.
- [8] Y. Shen, Y. Ren, A. T. Kristensen, A. Balatsoukas-Stimming, X. You, C. Zhang, and A. P. Burg, "Fast sequence repetition node-based successive cancellation list decoding for polar codes," in *Proc. IEEE Int. Conf. Commun. (ICC)*, 2022, pp. 1–7.
- [9] Y. Ren, A. T. Kristensen, Y. Shen, A. Balatsoukas-Stimming, C. Zhang, and A. P. Burg, "A sequence repetition node-based successive cancellation list decoder for 5G polar codes: Algorithm and implementation," *accepted by IEEE Trans. Signal Process.*, 2022.
- [10] A. Elkelesh, M. Ebada, S. Cammerer, and S. Ten Brink, "Belief propagation decoding of polar codes on permuted factor graphs," in *Proc. IEEE Wireless Commun. Net. Conf. (WCNC)*, 2018, pp. 1–6.
- [11] —, "Belief propagation list decoding of polar codes," *IEEE Commun. Lett.*, vol. 22, no. 8, pp. 1536–1539, Jun. 2018.
- [12] A. C and O. Gazi, "Noise-aided belief propagation list decoding of polar codes," *IEEE Commun. Lett.*, vol. 23, no. 8, pp. 1285–1288, May 2019.
- [13] Y. Ren, W. Xu, Z. Zhang, X. You, and C. Zhang, "Efficient belief propagation list decoding of polar codes," in *Proc. IEEE Int. Conf. ASIC (ASICON)*, 2019, pp. 1–4.
- [14] M. Geiselhart, A. Elkelesh, M. Ebada, S. Cammerer, and S. Ten Brink, "CRC-aided belief propagation list decoding of polar codes," in *Proc. IEEE Int. Symp. Inf. Theory (ISIT)*, 2020, pp. 395–400.
- [15] Y. Ren, Y. Shen, Z. Zhang, X. You, and C. Zhang, "Efficient belief propagation polar decoder with loop simplification based factor graphs," *IEEE Trans. Veh. Technol.*, vol. 69, no. 5, pp. 5657–5660, Mar. 2020.
- [16] B. Li, B. Bai, M. Zhu, and S. Zhou, "Improved belief propagation list decoding for polar codes," in *Proc. IEEE Int. Symp. Inf. Theory (ISIT)*, 2020, pp. 1–6.
- [17] N. Doan, S. A. Hashemi, M. Mondelli, and W. J. Gross, "On the decoding of polar codes on permuted factor graphs," in *Proc. IEEE Global Commun. Conf. (GLOBECOM)*, 2018, pp. 1–6.
- [18] B. Feng, R. Liu, and K. Tian, "A novel post-processing method for belief propagation list decoding of polar codes," *IEEE Commun. Lett.*, vol. 25, no. 8, pp. 2468–2471, Jun. 2021.
- [19] Y. Yu, Z. Pan, N. Liu, and X. You, "Belief propagation bit-flip decoder for polar codes," *IEEE Access*, vol. 7, pp. 10937–10946, Jan. 2019.
- [20] Y. Shen, W. Song, Y. Ren, H. Ji, X. You, and C. Zhang, "Enhanced belief propagation decoder for 5G polar codes with bit-flipping," *IEEE Trans. Circuits Syst. II*, vol. 67, no. 5, pp. 901–905, Mar. 2020.
- [21] Y. Shen, W. Song, H. Ji, Y. Ren, C. Ji, X. You, and C. Zhang, "Improved belief propagation polar decoders with bit-flipping algorithms," *IEEE Trans. Commun.*, vol. 68, no. 11, pp. 6699–6713, Aug. 2020.
- [22] H. Ji, Y. Shen, W. Song, Z. Zhang, X. You, and C. Zhang, "Hardware implementation for belief propagation flip decoding of polar codes," *IEEE Trans. Circuits Syst. I*, vol. 68, no. 3, pp. 1330–1341, Dec. 2020.
- [23] A. Balatsoukas-Stimming, P. Giard, and A. Burg, "Comparison of polar decoders with existing low-density parity-check and turbo decoders," in *Proc. IEEE Wireless Commun. Networking Conf. Workshops (WCNC)*, 2017, pp. 1–6.
- [24] A. Alamdar-Yazdi and F. R. Kschischang, "A simplified successive-cancellation decoder for polar codes," *IEEE Commun. Lett.*, vol. 15, no. 12, pp. 1378–1380, Dec. 2011.
- [25] G. Sarkis, P. Giard, A. Vardy, C. Thibault, and W. J. Gross, "Fast polar decoders: Algorithm and implementation," *IEEE J. Sel. Areas Commun.*, vol. 32, no. 5, pp. 946–957, May 2014.
- [26] M. Hanif and M. Ardakani, "Fast successive-cancellation decoding of polar codes: Identification and decoding of new nodes," *IEEE Commun. Lett.*, vol. 21, no. 11, pp. 2360–2363, Nov. 2017.
- [27] C. Condo, V. Bioglio, and I. Land, "Generalized fast decoding of polar codes," in *Proc. IEEE Glob. Comm. Conf. (Globecom)*, 2018, pp. 1–6.
- [28] H. Zheng, S. A. Hashemi, A. Balatsoukas-Stimming, Z. Cao, T. Koonen, J. Cioffi, and A. Goldsmith, "Threshold-based fast successive-cancellation decoding of polar codes," *IEEE Trans. Commun.*, vol. 69, no. 6, pp. 3541–3555, Jun. 2021.
- [29] X. You, C.-X. Wang, J. Huang *et al.*, "Towards 6G wireless communication networks: Vision, enabling technologies, and new paradigm shifts," *Sci. China Inf. Sci.*, vol. 64, no. 1, pp. 1–74, 2021.
- [30] Y. S. Park, Y. Tao, S. Sun, and Z. Zhang, "A 4.68Gb/s belief propagation polar decoder with bit-splitting register file," in *Proc. IEEE Symp. VLSI Circuits Digest Techn. Papers (VLSIC)*, 2014.
- [31] S. Jing, J. Yang, A. Yu, X. You, and C. Zhang, "Graph-merged detection and decoding of polar-coded MIMO systems," in *Proc. Int. Conf. Wireless Commun. Signal Process. (WCSP)*, 2017.
- [32] A. Jalali and Z. Ding, "Joint detection and decoding of polar coded 5G control channels," *IEEE Trans. Wireless Commun.*, vol. 19, no. 3, pp. 2066–2078, Jan. 2020.
- [33] N. Hussami, S. B. Korada, and R. Urbanke, "Performance of polar codes for channel and source coding," in *Proc. IEEE Int. Symp. Inf. Theory (ISIT)*, 2009, pp. 1488–1492.
- [34] A. Pamuk, "An FPGA implementation architecture for decoding of polar codes," in *Proc. IEEE Int. Symp. Wireless Commun. Syst. (ISWCS)*, 2012, pp. 437–441.
- [35] B. Yuan and K. K. Parhi, "Early stopping criteria for energy-efficient low-latency belief-propagation polar code decoders," *IEEE Trans. Signal Process.*, vol. 62, no. 24, pp. 6496–6506, Dec. 2014.
- [36] J. Yang, C. Zhang, H. Zhou, and X. You, "Pipelined belief propagation polar decoders," in *Proc. IEEE Int. Symp. Circuits Syst. (ISCAS)*, 2016, pp. 413–416.
- [37] S. Sun and Z. Zhang, "Architecture and optimization of high-throughput belief propagation decoding of polar codes," in *Proc. IEEE Int. Symp. Circuits Syst. (ISCAS)*, 2016, pp. 1–4.
- [38] S. M. Abbas, Y. Fan, J. Chen, and C.-Y. Tsui, "High-throughput and energy-efficient belief propagation polar code decoder," *IEEE Trans. VLSI Syst.*, vol. 25, no. 3, pp. 1098–1111, Nov. 2017.
- [39] Y. Chen, W. Sun, C. Cheng, T. Tsai, Y. Ueng, and C. Yang, "An integrated message-passing detector and decoder for polar-coded massive MU-MIMO systems," *IEEE Trans. Circuits Syst. I*, vol. 66, no. 3, pp. 1205–1218, Nov. 2019.
- [40] M. Geiselhart, A. Elkelesh, J. Clausius, and S. Ten Brink, "A polar subcode approach to belief propagation list decoding," *arXiv preprint arXiv:2205.06631*, 2022.
- [41] V. E. Beneš, "Optimal rearrangeable multistage connecting networks," *Bell system technical journal*, vol. 43, no. 4, pp. 1641–1656, Jul. 1964.
- [42] D. Oh and K. K. Parhi, "Low-complexity switch network for reconfigurable ldpc decoders," *IEEE Trans. VLSI Syst.*, vol. 18, no. 1, pp. 85–94, Mar. 2010.
- [43] M. Geiselhart, A. Elkelesh, M. Ebada, S. Cammerer, and S. Ten Brink, "Automorphism ensemble decoding of Reed–Muller codes," *IEEE Trans. Commun.*, vol. 69, no. 10, pp. 6424–6438, Jul. 2021.
- [44] V. Bioglio, I. Land, and C. Pillet, "Group properties of polar codes for automorphism ensemble decoding," *arXiv preprint arXiv:2206.03342*, 2022.
- [45] B.-S. Su, C.-H. Lee, and T.-D. Chiuhe, "A 58.6/91.3 pJ/b dual mode belief propagation decoder for LDPC and polar codes in the 5G communications standard," *IEEE Solid State Circuits Letter*, vol. 5, pp. 98–101, 2022.
- [46] *5G NR: Multiplexing and channel coding*, 3GPP Technical Specification 38.212 Version 15.2.0, Jul. 2018.
- [47] A. Elkelesh, M. Ebada, S. Cammerer, and S. Ten Brink, "Decoder-tailored polar code design using the genetic algorithm," *IEEE Trans. Commun.*, vol. 67, no. 7, pp. 4521–4534, Apr. 2019.
- [48] F. Kschischang, B. Frey, and H.-A. Loeliger, "Factor graphs and the sum-product algorithm," *IEEE Trans. Inf. Theory*, vol. 47, no. 2, pp. 498–519, Feb. 2001.
- [49] E. Arkan, "Polar codes: a pipelined implementation," in *Int. Symp. Broad. Commun. (ISBC)*, 2010, pp. 11–14.
- [50] W. Xu, X. Tan, Y. Be'ery, Y.-L. Ueng, Y. Huang, X. You, and C. Zhang, "Deep learning-aided belief propagation decoder for polar codes," *IEEE J. Emer. Top. Circuits Syst.*, vol. 10, no. 2, pp. 189–203, May 2020.
- [51] Y. Ren, C. Zhang, X. Liu, and X. You, "Efficient early termination schemes for belief-propagation decoding of polar codes," in *Proc. IEEE Int. Conf. on ASIC (ASICON)*, 2015, pp. 1–4.
- [52] A. Balatsoukas-Stimming, M. Bastani Parizi, and A. Burg, "LLR-based successive cancellation list decoding of polar codes," *IEEE Trans. Signal Process.*, vol. 63, no. 19, pp. 5165–5179, Oct. 2015.
- [53] S. Sun and Z. Zhang, "Architecture and optimization of high-throughput belief propagation decoding of polar codes," in *Proc. IEEE Int. Symp. Circuits Syst. (ISCAS)*, 2016, pp. 165–168.
- [54] F. Ercan, T. Tonnellier, and W. J. Gross, "Energy-efficient hardware architectures for fast polar decoders," *IEEE Trans. Circuits Syst. I*, vol. 67, no. 1, pp. 322–335, Oct. 2020.